Conference Proceedings

EuroSun 2016
Palma de Mallorca (Spain), 11 - 14 October 2016

Optimization Methods for Optimal Power Flow in Microgrid Non-Autonomous Mode

Luis O. Polaco Vasquez[1], Cristian A. Carreño Meneses[1], Alejandro Pizano Martínez[1], Juana López Redondo[2], Manuel Pérez García[2] and José Domingo Álvarez Hervás[2]

[1] University of Guanajuato, Irapuato-Salamanca Campus, Guanajuato (Mexico)

[2] University of Almería, Agrifood Campus of International Excellence (ceiA3)
CIESOL Joint Centre University of Almería -CIEMAT, Almería (Spain)

Abstract

In this work, the Optimal Power Flows (OPF) for the tertiary control problem in microgrid is studied. The objective is to find the optimal dispatch of energy which maximize the benefit. Such energy can come from renewable sources, storage devices or the main power grid. To this aim, a unified model of the microgrid, which is operated in non-autonomous mode, has been developed. This model is composed by basic submodels of the distribution system, the photovoltaic panels, the wind turbines and the batteries for energy storage. The optimization problem is solved using three different methods provided by the optimization toolbox of MATLAB®. More precisely, an interior point method, a genetic algorithm and the direct search method have been considered. The performance of those optimization methods is analyzed in terms of efficiency and effectiveness. Some good results are depicted. The case study considers the microgrid connected to the main power system with the photovoltaic panels, the wind turbines and the batteries for energy storage. In this test, the power supplied by the grid is mostly due to the size of each renewable source, but it is possible to see the contribution of the microgrid in the cost graphics.

Keywords: *optimal power flow, microgrid, distributed power systems*

1. Introduction

Nowadays the electricity sector worldwide is subject to meet strict environmental policies that promote the use of renewable energy sources, with the aim to contribute with the environmental and global energy sustainability. The operation modes of a microgrid are two: i) non-autonomous (connected to the main power grid) and, ii) autonomous (not connected to the main power grid) [Olivares, 2014]. In any of these operation modes, the microgrid is controlled through a three-level hierarchical control system which can be split in a primary controller, a secondary controller and tertiary one [Bidram, 2012]. This work is part of the tertiary controller of the microgrid operating in non-autonomous mode. In this scenario, the objectives that are mainly considered for the tertiary controller are the minimization of the energy cost from the main grid and the optimization of the voltages profile within the microgrid among others, through different optimization methods [Katiraei, 2008]. As a result, Optimal Power Flows (OPF) analysis is the cornerstone of the tertiary controller. Taken it into account, this paper is particularly focused in implement a model of optimal power flows of the microgrid for non-autonomous operating mode and three different optimization methods for the resolution of OPF. Based on the profiles of electric demand curves and solar radiation from the cities of Salamanca and Guanajuato, Mexico, and the predicted wind speed for a period of time T, the analysis of optimal power flows can be used to determine the optimum dispatch for the energy storage devices and the optimal quantity of power imported from the main grid, with the aim of maximizing the benefit of the energy generated by the Distributed Energy Sources (DES) installed in the microgrid and, at the same time, reducing the cost of the energy imported from the main grid [Levron, 2013]. In a microgrid framework,

doi:10.18086/eurosun.2016.08.24 Available at http://proceedings.ises.org

different models of optimal power flow, optimization algorithms and strategies for the energy management have been proposed [Olivares et al 2014, Levron et al 2013, Gill et al 2014]. Despite this, there is not any strategy of optimal power flows that can be considered as the ultimate tool for the implementation of a tertiary controller. Therefore, the problem of optimal flows for microgrids is a topic of current research and of relevant importance in this context.

This work presents three different optimization methods for a unified model of optimal power flow for microgrids, which considers basic models of the elements of the distribution system, photovoltaic panels, wind turbines, as well as batteries for energy storage. The model is solved by three different methods of optimization: i) interior point, ii) genetic algorithm and, iii) direct search provided by the optimization toolbox included in MATLAB®. The solutions obtained allows us to evaluate the optimal dispatch of energy storage devices and the optimal amount of power imported from the main grid. The mathematical basis of this work and the generic model of OPF for microgrid are presented in the Section 2. Section 3 shows the mathematical models of the different components of the microgrid as a wind turbine, photovoltaic module, battery, load, and the components of the distribution lines. In Sections 4 and 5 the explicit model of OPF and its solution are described, respectively. In Section 6 are described, showed and compared the results obtained with the different methods of optimization for the proposed case study. Finally, the conclusions of this work are presented in Section 7.

2. Generic model of OPF for Microgrid

For electric demand curves, solar radiation and predicted wind speed for an interval of time T, the general model of OPF is given by eqs. 1-4. It should be noted that, in this model, it is considered that the period of time T is composed of a set of time stages t_z ($\forall z = 1,..., end$), such that $T = [t_1,..., t_{end}]$.

$$\text{Minimize} \quad F_T = \sum_{t_z=1}^{t_{end}} f^{t_z}(\boldsymbol{y}^{t_z}) \qquad \text{(eq. 1)}$$

$$\text{Subject to} \quad \boldsymbol{h}^{t_z}(\boldsymbol{y}^{t_z}) = \boldsymbol{0} \;;\; \forall t_z \in T \qquad \text{(eq. 2)}$$

$$\boldsymbol{g}^{t_z}(\boldsymbol{y}^{t_z}) \leq \boldsymbol{0} \;;\; \forall t_z \in T \qquad \text{(eq. 3)}$$

$$\underline{\boldsymbol{y}} \leq \boldsymbol{y}^{t_z} \leq \overline{\boldsymbol{y}} \;;\; \forall t_z \in T \qquad \text{(eq. 4)}$$

Taking into account that, t_z represents the *z-th* time stage, the description of the terms of the model, eqs. 1-4, is as follows: F_T is the objective function to optimize along the interval T, $\boldsymbol{h}(\boldsymbol{y})$ is a set of equality constraints, which represents the balance equations of active power and reactive on all the nodes in the microgrid, as well as other operating conditions that must be fulfilled unconditionally, $\boldsymbol{g}(\boldsymbol{y})$ is a set of constraints of inequalities that represents the physical limits and operating of the elements that make up the microgrid, $\boldsymbol{y}$ is the set of decision variables (to be optimized) composed of subsets $\boldsymbol{y}_{RD}$, $\boldsymbol{y}_{MF}$ and $\boldsymbol{y}_B$ such $\boldsymbol{y}=[\boldsymbol{y}_{RD}, \boldsymbol{y}_{MF}, \boldsymbol{y}_B,]$. Where $\boldsymbol{y}_B$, $\boldsymbol{y}_{RD}$ and $\boldsymbol{y}_{MF}$ represent batteries variables, distribution grid and photovoltaic modules, respectively. The upper and lower limits, $\overline{\mathbf{y}}$ and $\underline{\mathbf{y}}$, of these variables are formulated through the inequality constraints, see eq. 4.

3. Model for microgrids components

The models for microgrid components presented in this section are considered to formulate explicitly the unified model of OPF for microgrid presented in Section 4.

3.1. Points of Common Coupling

It is considered that the microgrid operates in non-autonomous mode, such that is connected to the main grid in N_{pac} ($N_{pac} \geq 1$) Points of Common Coupling (PCC). It is assumed that each PCC is electrically robust and is an interface for the unlimited exchange of both, active and reactive power between the microgrid and the main grid. In this context, the PCC are modeled as generation sources that operate at voltage levels

magnitude $V_j^{t_z}$ and angle $\theta_j^{t_z}$ within the limits given by eq. 5:

$$\left.\underline{V}_j \le V_j^{t_z} \le \overline{V}_j ; \underline{\theta}_j \le \theta_j^{t_z} \le \overline{\theta}_j \right\} \ \forall t_z \in T \ \ ; \ \ \forall j \in PAC \qquad \text{(eq. 5)}$$

For time t_z, the cost of active total power exchanged through the PCC is modeled by eq. 6. Where a_j, b_j and c_j are weight constant coefficients for the *j-th* PCC. The variable $P_{RPj}^{t_z}$ means the power exchanged through the *j-th* PCC. The decision variables associated with the PCC are $\left[V_j^{t_z}, \theta_j^{t_z}, P_{RPj}^{t_z}\right] \in \boldsymbol{y}_{RD}$ ($\forall t_z \in T, \forall j \in PCC$).

$$f^{t_z}(\boldsymbol{y}^{t_z}) = \sum_{j=1}^{N_{pac}} a_j + b_j (P_{RPj}^{t_z}) + c_j (P_{RPj}^{t_z})^2 \ ; \ \forall t_z \in T \qquad \text{(eq. 6)}$$

3.2. Feeders

Each feeder is modeled as a line of transmission, as is illustrated in Fig. (1) Where $\boldsymbol{I}_i$ and $\boldsymbol{E}_i$ are the phasors of the injected electricity and voltage, respectively, on the node i ($i = k,m$) of the microgrid. R, L and B_c represent the parameters of resistance series, inductance series and shunt susceptance, respectively, of the feeder. The relationship electricity-voltage of the equivalent circuit is given by eq. 9 [Acha, 2004]. Where admittance matrix elements are evaluated in eq. 8 and eq. 9.

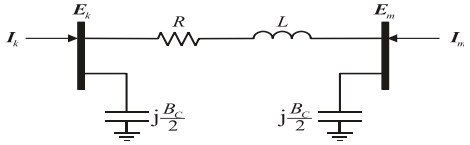

Fig. 1: π circuit for the feeders

$$\begin{bmatrix} \boldsymbol{I}_k^{t_z} \\ \boldsymbol{I}_m^{t_z} \end{bmatrix} = \begin{bmatrix} \boldsymbol{Y}_{kk} & \boldsymbol{Y}_{km} \\ \boldsymbol{Y}_{mk} & \boldsymbol{Y}_{mm} \end{bmatrix} \begin{bmatrix} \boldsymbol{E}_k^{t_z} \\ \boldsymbol{E}_m^{t_z} \end{bmatrix} \quad \forall t_z \in T \qquad \text{(eq. 7)}$$

$$\boldsymbol{Y}_{kk} = \boldsymbol{Y}_{mm} = (\boldsymbol{y}_{km} + j0.5Bc) = G_{kk} + jB_{kk} ; \boldsymbol{Y}_{km} = \boldsymbol{Y}_{mk} = -\boldsymbol{y}_{km} = G_{km} + jB_{km} \qquad \text{(eq. 8)}$$

$$G_{km} = R/R^2 + (\omega L)^2 ; B_{km} = -\omega L/R^2 + (\omega L)^2 \qquad \text{(eq. 9)}$$

Starting from Fig. 1 and eq. 7 it is possible to obtain expressions that model the injection of active and reactive power, eq. 10 and eq. 11 respectively, on the node i ($i = k, m$) at each moment $t_{T \in} z$ [Acha, 2004]. Where $j = k, m$, being $j \neq i$. The variables $V_n^{t_z}$ and $\theta_n^{t_z}$ ($n=i, j$) represent the magnitude and the angle of the nodal voltage phasor $\boldsymbol{E}_i$.

$$P_{inyi}^{t_z} = (V_i^{t_z})^2 G_{ii} + V_i^{t_z} V_j^{t_z} \left[G_{ij} Cos(\theta_i^{t_z} - \theta_j^{t_z}) + B_{ij} Sin(\theta_i^{t_z} - \theta_j^{t_z}) \right] \qquad \text{(eq. 10)}$$

$$Q_{nyi}^{inj\ t_z} = -(V_i^{t_z})^2 B_{ii} + V_i^{t_z} V_j^{t_z} \left[G_{ij} Sin(\theta_i^{t_z} - \theta_j^{t_z}) - B_{ij} Cos(\theta_i^{t_z} - \theta_j^{t_z}) \right] \qquad \text{(eq. 11)}$$

The decision variables associated to these feeders correspond to the nodal voltages in its terminals $\left[V_k^{t_z}, V_m^{t_z}, \theta_k^{t_z}, \theta_m^{t_z}\right] \in \boldsymbol{y}_{RD}$ ($\forall t_z \in T$).

3.3. Transformer

The primary winding is considered an ideal transformer with relation of complex tap T_v:1 and T_i:1 in series with the impedance Z_p (refers to Fig. (2)). Where $\boldsymbol{T}_v = \boldsymbol{T}_i^* = T_v \angle \phi_{tv}$, the symbol * denotes complex conjugate. The secondary winding is also represented as an ideal transformer with relation of complex tap $\boldsymbol{U}_v$:1 and $\boldsymbol{U}_i$:1 in series with the impedance $\boldsymbol{Zs}$. Where $\boldsymbol{U}_v = \boldsymbol{U}_i^* = U_v \angle \phi_{uv}$. The relationship between voltage $\boldsymbol{V}_p$ and electricity $\boldsymbol{I}_p$ of the primary winding and the voltage $\boldsymbol{V}_s$ and electricity $\boldsymbol{I}_s$ of the secondary one is given by eq. 12 [Acha, 2004].

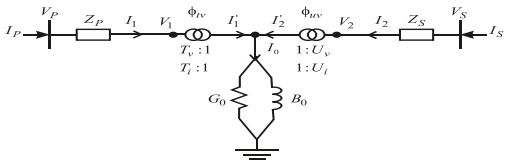

Fig. 2: T model for the transformers

$$\begin{bmatrix} \boldsymbol{I}_p^{t_z} \\ \boldsymbol{I}_s^{t_z} \end{bmatrix} = \left[\begin{bmatrix} G_{PP}\ G_{PS} \\ G_{SP}\ G_{SS} \end{bmatrix} + j \begin{bmatrix} B_{PP}\ B_{PS} \\ B_{SP}\ B_{SS} \end{bmatrix} \right] \begin{bmatrix} \boldsymbol{V}_p^{t_z} \\ \boldsymbol{V}_s^{t_z} \end{bmatrix};\ \forall t_z \in T \qquad \text{(eq. 12)}$$

where:

$$G_{PP} = \frac{F1(U_v^2 + R1) + F2R2}{F1^2 + F2^2},\ B_{PP} = \frac{F1R2 - F2(U_v^2 + R1)}{F1^2 + F2^2}$$

$$G_{SS} = \frac{F1(T_v^2 + R3) + F2R4}{F1^2 + F2^2},\ B_{SS} = \frac{F1R4 - F2(T_v^2 + R3)}{F1^2 + F2^2}$$

As the feeders, the injections of active and reactive power in the connection nodes *i* and *j*, where *i = p, s; j = p, s; i≠j,* are represent by eqs. 10 and 11, but considering the conductance and susceptance matrices of eq. 12. It is important to highlight that, the decision variables associated with transformers correspond to the nodal voltages in its terminals $\left[V_p^{t_z}, V_s^{t_z}, \theta_p^{t_z}, \theta_s^{t_z}\right] \in \boldsymbol{y}_{RD}$. ($\forall t_z \in T$).

3.4. Batteries

The batteries are elements that can operate in charge or discharge mode to provide or consume a net amount of active power in their connection node. Then, the *j-th* battery is represented by two sources of active power, as shown in Fig. 3 [Gill, 2014]. One of them represents the charge power $P_{Bc\,j}^{t_z} \leq 0$ and the other the discharge power $P_{Bd\,j}^{t_z} \geq 0$, the sum of both powers represents the net power $P_{Bn\,j}^{t_z}$ provided or consumed by the battery in their connection node.

$$P_{Bn\,j}^{t_z} = P_{Bc\,j}^{t_z} + P_{Bd\,j}^{t_z};\ 0 \leq P_{Bd\,j}^{t_z};\ P_{Bc\,j}^{t_z} \leq 0;\ \forall t_z \in T \qquad \text{(eq. 13)}$$

In addition, the voltage phasor in the connection node is represented by its magnitude $V_j^{t_z}$ and its angle $\theta_j^{t_z}$. Thus, the decision variables of the *j-th* battery are $\left[P_{Bd\,j}^{t_z}, P_{Bc\,j}^{t_z}\right] \in \boldsymbol{y}_B$ ($\forall t_z \in T$), while $[V_j^{t_z}, \theta_j^{t_z}] \in \boldsymbol{y}_{RD}$ ($\forall t_z \in T$). Moreover, the State Of Charge of the *j-th* battery (SOC) in the time t_z ($SOC_{B\,j}^{t_z}$) can be approximated by means of eq. 14.

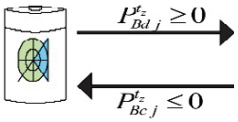

Fig 3. Battery model

$$SOC_{B\,j}^{t_z} = SOC_{B\,j}^{t_0} - \frac{\varepsilon_{c\,j}\Delta t}{E_{Bnom\ j}} \sum_{t=1}^{t_z} P_{Bc\,j}^{t} - \frac{\Delta t}{E_{Bnom\ j}\,\varepsilon_{d\,j}} \sum_{t=1}^{t_z} P_{Bd\,j}^{t} \qquad \text{(eq. 14)}$$

It is assumed that the energy provided by the batteries has not cost, since it is absorbed and provided in the same node of connection. However, since the optimization algorithm will manage the power, batteries will be charged in periods of low-cost energy and it will be discharged in periods of high cost. This fact involves an economic benefit in the operation of the microgrid.

3.5. Wind turbine

For the aim of the stationary analysis, the wind turbine can be considered like a source of non controlled

active power $P_{Aj}^{t_z}$, depending on its density δ_w, wind speed $S_w^{t_z}$, as well as of the area A_w covered by the blades of the wind turbine [Wang, 2009]

$$P_{Aj}^{t_z} = \delta_w A_w \left(S_w^{t_z}\right)^3 \Big/ 2, \forall t_z \in T \qquad \text{(eq. 15)}$$

Since it is considered that the power delivered by the wind turbine is not controllable; this element does not introduce decision variables. However, eq. 16 is required to assess the contribution of the power *j-th* of the wind turbine for a wind speed curve, $S_w^{t_z}\ \forall\ t_z \in T$, density, δ_w, and area, A_w, given. Clearly, the magnitude $V_j^{t_z}$ and angle $\theta_j^{t_z}$ of the voltage phasor of the connection node are considered as decision variables, such that $[V_j^{t_z}, \theta_j^{t_z}] \in \boldsymbol{y}_{RD}$ ($\forall t_z \in T$). Finally, it is assumed that the energy provided by the wind turbine has no cost. In addition, it is considered available a good forecast for wind speed curves.

3.6. Photovoltaic modules

Figure 4 shows the schematic model of a photovoltaic module connected to the node *k-th* through a converter DC/AC 4 [Bellini, 2009]. The implicit expression eq. 16 models the behavior of the current DC in $I_{CD\,k}^{t_z}$ panel terminals. Where I_{ph}, I_0, $V_{CD\,k}^{t_z}$, R_s, n_s and n_p represent the current of the panel photovoltaic, the current of saturation, the DC voltage in the module terminals, the resistance in series, and the number of cells in series and in parallel, respectively. The term R_s is evaluated from eq. 17, where V_{oc}, V_{mp}, I, I_{mp} represent the open circuit voltage, the voltage of the point of maximum power, short circuit electricity and maximum power point electricity, respectively. Terms I_{sc} and V_{oc} are evaluated through eq. 18 and eq. 19, respectively. Where $I_{sc,\,stc}$, G, G_{stc}, k_i, T, T_{stc}, $V_{oc,\,stc}$, and k_v represent the short circuit electricity standard under conditions of test, irradiance under test, electricity temperature coefficient, temperature of the panel, standard temperature under test, standard low open circuit voltage conditions test and voltage and temperature coefficient, respectively.

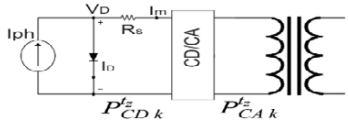

Fig. 4 Schematic model of a photovoltaic module

$$I_{CDk}^{t_z} = \left[I_{ph} - I_0 \left(\exp\left(\frac{\frac{V_{CD\,k}^{t_z}}{n_s} + \frac{I_{CDk}^{t_z}}{n_p} R_s}{V_{CD}^{t_z}} \right) - 1 \right) \right] n_p; \forall t_z \in T \qquad \text{(eq. 16)}$$

$$R_s = \frac{\frac{V_{oc} - V_{mp}}{n_s} + V_{CD}^{t_z} \ln\left(\frac{I_{sc} - I_{mp}}{I_{sc}}\right)}{\frac{I_{mp}}{n_p}} \qquad \text{(eq. 17)}$$

$$I_{sc}(T, G) = I_{sc,stc} - \frac{G}{G_{stc}} \left[1 + \frac{k_i}{100} (T - T_{stc}) \right] \qquad \text{(eq. 18)}$$

$$V_{oc}(T) = V_{oc,stc} \left[1 + \frac{k_v}{100} (T - T_{stc}) \right] \qquad \text{(eq. 19)}$$

In this work, the photovoltaic module parameters involved in eqs.16-19 were taken from the features of the polycrystalline module Solartec S60PC-250 [Bellini, 2009]. Moreover, a good forecast of solar irradiance curves is considered available.

According to the model of the Fig. 4, the injected power in DC terminals (generated by module) can be expressed directly as:

$$P_{CD\,k}^{t_z}\left(V_{CD\,k}^{t_z},\, I_{CD\,k}^{t_z}\right) = I_{CD\,k}^{t_z} V_{CD\,k}^{t_z};\ \forall t_z \in T \qquad \text{(eq. 20)}$$

Moreover, the balance of power between the terminals of AC and DC of the inverter must also be fulfilled. If the losses of the converter are rejected:

$$P_{CA\,k}^{t_z}\left(V_k^{t_z}, V_m^{t_z}, \theta_k^{t_z}, \theta_m^{t_z}\right) = P_{CD\,k}^{t_z}\left(V_{CD\,k}^{t_z}, I_{CD\,k}^{t_z}\right);\ \forall t_z \in T \qquad \text{(eq. 21)}$$

where $P_{CA\,k}^{t_z}$ is the active power injected at the terminals of the primary transformer coupling module. $V_k^{t_z}$ and $\theta_k^{t_z}$ are the magnitude and the angle, respectively, of the voltage phasor for such terminals. $V_m^{t_z}$ and $\theta_m^{t_z}$ represent the same but for the secondary terminals. Therefore, $P_{CA\,k}^{t_z}$ in eq. 21 is formulated explicitly by means of eq. 11, but considering the matrix of conductances and susceptances of eq. 13. It is important to mention that, due to it is considered a DC/AC converter multipulse with 48 pulses, the following relationship must also keep [Zúñiga, 2006]:

$$V_{CD\,k}^{t_z} = \frac{\pi}{16} V_k^{t_z};\ \forall t_z \in T \qquad \text{(eq. 22)}$$

It is important to highlight that, the decision variables introduced by the photovoltaic module are $\left[V_{CD\,k}^{t_z} I_{CD\,k}^{t_z}\right] \in \boldsymbol{y}_{MF}$ ($\forall t_z \in T$), whereas $[V_k^{t_z}, V_m^{t_z}, \theta_k^{t_z}, \theta_m^{t_z}] \in \boldsymbol{y}_{RD}$ ($\forall t_z \in T$).

3.7. Electrical load

Energy consumption in load nodes of the microgrid is represented by a model of constant power for any interval of time T. The power *i-th* $\boldsymbol{S}_{li}^{t_z}$ complex consumed in the node is then represented by eq. 23. Where $P_{li}^{t_z}$ and $Q_{li}^{t_z}$ represent the power consumption active on that node at the instant t_z, respectively.

$$\boldsymbol{S}_{li}^{t_z} = P_{li}^{t_z} + jQ_{li}^{t_z}\ \ \forall t_z \in T \qquad \text{(eq. 23)}$$

Model of energy demand does not introduce decision variables to the optimization problem, but the magnitude $V_i^{t_z}$ and angle $\theta_i^{t_z}$ of the connection node phasor voltage must be considered as decision variables, such as $[V_i^{t_z}, \theta_i^{t_z}] \in \boldsymbol{y}_{RD}$ ($\forall t_z \in T$). In addition, it is considered that a good forecast of the energy demand curves is available ($\boldsymbol{S}_{li}^{t_z} \forall i, t_z \in T$).

4. Explicit model of OPF

Models of the microgrid components described in Section 3 are considered in this section to formulate explicit model of OPF for non-autonomous microgrid. For this purpose, is considered one generic microgrid composed of a number of N_{bAC} nodes in AC, N_{bCD} nodes in DC, N_{Al} feeders, N_T transformers, N_B battery, N_A wind turbines, N_{MF} photovoltaic modules and N_{CE} electrical loads. Noted that, the N_{pac} points of common coupling are a subset of the N_{bAC} nodes in AC. In addition, the nodes in DC represent DC terminals of the photovoltaic modules, such N_{bCD}=N_{MF}.

4.1. Objective function

The intention is to minimize eq. 1, which is formulated explicitly taking into account eq. 6, as follows:

$$F_T = \sum_{t_z=1}^{t_{end}} \sum_{j=1}^{N_{pac}} a_j + b_j\ (P_{RP\,j}^{t_z}) + c_j\ (P_{RP\,j}^{t_z})^2 \qquad \text{(eq. 24)}$$

Note that eq. 24 denotes that the objective is to minimize the cost of the total energy imported through the PCC during the period of time T to supply the demand curves predicted $\boldsymbol{S}_{li}^{t_z} \forall i, t_z \in T$.

4.2. Equality constraints

The set of equality constraints **h(y)** in eq. 2 is expressed explicitly as follows. The constraints of power active, $\Delta P_{RDi}^{t_z}$, and reactive, $\Delta Q_{RDi}^{t_z}$, balance corresponding to the nodes of the microgrid in AC are written in the first block of eq. 25.

$$\boldsymbol{h}^{t_z}(\boldsymbol{y}^{t_z})=\left\{\begin{array}{c}\left.\begin{array}{c}\Delta P^{t_z}_{RD\,i}=P^{t_z}_{RP\,i}+\sum_{\forall j\in i}P^{t_z}_{Bc\,j}+\sum_{\forall j\in i}P^{t_z}_{Bd\,j}+\sum_{\forall j\in i}P^{t_z}_{A\,j}+\\ \sum_{\forall j\in i}P^{t_z}_{CD\,j}-\sum_{\forall j\in i}P^{t_z}_{lj}-\sum_{\forall j\in i\,|\,j\in N_{AI},N_T}P^{t_z}_{inj\,j}(\boldsymbol{V},\boldsymbol{\theta})=0,\\ \Delta Q^{t_z}_{RD\,k}=-\sum_{\forall j\in k}Q^{t_z}_{lj}-\sum_{\forall j\in k}Q^{t_z}_{inj\,j}(\boldsymbol{V},\boldsymbol{\theta})=0\\ i=1,2,\ldots,N_{bAC}\;;\;k=1,2,\ldots,N_{bAC}\,|\,\forall k\notin N_{GEN}\end{array}\right\}\\ \left.\begin{array}{c}\Delta I^{t_z}_{CD\,k}=I^{t_z}_{CD\,k}-f_{CD}(V^{t_z}_{CD\,k},I^{t_z}_{CD\,k})=0,\\ \Delta P^{t_z}_{CD\,k}=P^{t_z}_{CAk}(\boldsymbol{V},\boldsymbol{\theta})-P^{t_z}_{CD\,k}(V^{t_z}_{CD\,k},I^{t_z}_{CD\,k})=0,\\ \Delta V^{t_z}_{CD\,k}=V^{t_z}_{CD\,k}-(\pi/16)V^{t_z}_{k}=0\\ k=N_{bAC}+1,\ldots,N_{bAC}+N_{bCD}\end{array}\right\}\forall t_z\in T\end{array}\right. \qquad \text{(eq. 25)}$$

4.3. Inequality constraints functions

According to the elements models introduced in Section 3, the only inequality constraints function $\boldsymbol{g}(\boldsymbol{y})$ in eq. 3 corresponds to the batteries, as follows. The batteries have finite capacity of charge and discharge. With this point in mind, the SOC is modulated over the period of time T through eq. 26 [Gill, 2014].

$$\boldsymbol{h}^{t_z}(\boldsymbol{y}^{t_z})=\left\{SOC^{\min}_{B\,j}\le SOC^{t_z}_{B\,j}\le SOC^{\max}_{B\,j}\right\}_{\forall j\in N_B;\forall t_z\in T} \qquad \text{(eq. 26)}$$

4.4. Equality constraints variables

Should be taken into account that, the decision variables must acquire admissible values, otherwise, the solution provided by the OPF model could not make sense from a practical point of view. For this reason, the decision variables $\boldsymbol{y}$ are limited during the interval of time T by means of the constraints set in eq. 27.

$$\left\{\begin{array}{c}\underline{\boldsymbol{y}}_{RD}\le\boldsymbol{y}^{t_z}_{RD}\le\overline{\boldsymbol{y}}_{RD}\\ \underline{\boldsymbol{y}}_{MF}\le\boldsymbol{y}^{t_z}_{MF}\le\overline{\boldsymbol{y}}_{MF}\\ \underline{\boldsymbol{y}}_{B}\le\boldsymbol{y}^{t_z}_{B}\le\overline{\boldsymbol{y}}_{B}\end{array}\right\}_{\forall t_z\in T} \qquad \text{(eq. 27)}$$

5. Solution of the OPF model

The OPF model eqs. 24-27 corresponds to a non-linear optimization model with constraints, which could be not continuous or differentiable. For this reason, is solved by means of three different optimization methods provided by MATLAB® optimization toolbox. The methods are: i) interior point method, ii) genetic algorithm and, iii) direct search method. For this purpose, the objective function, eq. 24, and the constrains, eqs. 25-27, are written in two separate functions, which are provided as input arguments to the above-mentioned functions. For the interested reader a detailed description of the use of these tools can be found in [MathWorks et al 2002, MathWorks et al 2013].

5.1. Interior Point Method

The interior point method is applied through the *fmincon* function which belongs to the MATLAB® 'Optimization Toolbox' [MathWorks, 2002]. It is considered as a tool for local search with constraints for non-linear multivariable functions. Therefore, it fits well for the OPF problem in microgrids.

5.2. Direct Search Method

The direct search method is applied through the function *patternsearch* which belongs to the MATLAB® 'Direct Search and Genetic Algorithm Toolbox' [MathWorks, 2013] and, like *fmincon*, can be classified as a tool for local search with non-linear constraints for multivariate functions such as the OPF problem in microgrids.

5.3. Genetic Algorithm Method

The genetic algorithm method is applied through of the *ga* function which belongs to the MATLAB® 'Direct Search and Genetic Algorithm Toolbox' and is especially thought for the optimization of global non-linear problems with or without constraints. Also, provides a great flexibility since contains multiple parameters of configuration.

6. Results

In this section, the analysis of optimal power flows for the microgrid showed in Fig. 5 is presented with the aim of showing and comparing the different optimization methods used in this work. The microgrid is connected to the main grid through the only PCC (node 1). Note that, the elements of the network between pair of nodes 1-2, 3-6, 4-7 and 5-8 are transformers. The other elements are feeders. The parameters of the network distribution models, photovoltaic module, wind turbine components, as well as the cost coefficients of associated at the energy import are presented in the Appendix. For the case of study has been considered the unit variables in per unit (pu), for which it took a base power and voltage of 100 VA and 100 V, respectively.

For the analysis, the forecasted curves of active power demand, wind speed and solar irradiation from the city of Salamanca (Mexico) are considered. These signals are displayed in Fig. 6a, 6b and 6c, respectively, and were provided by the Center for Atmospheric Sciences of the University of Guanajuato. The limits of the magnitudes for the AC voltage for all nodes in the microgrid are 0.95≤V≤1.05 pu. The limits of batteries SOC are 0.2 ≤SOC (t_z) ≤0.95 (in %) while the initial SOC is $SOC(t_0)$ = 0.2 (in %). The results, which have been obtained with a PC DELL with 8 GB of RAM and an Intel processor i5 - 3230 M CPU @ 2.40 GHz, from the solution of the OPF model are shown and discussed below.

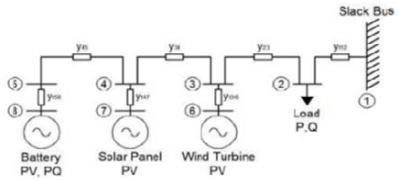

Fig. 5 Microgrid scheme

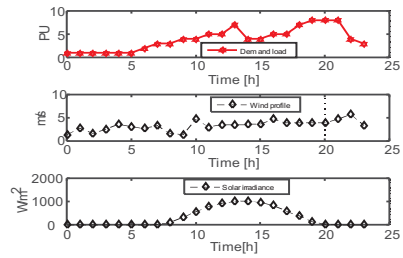

Fig. 6 Forecasted signals: a) active power demand, b) wind speed, c) solar irradiance

Figure 7a shows the active power provided by the battery, wind turbine, module PV and the imported one from the main grid. There is a greater percentage of the demand curve, see Fig. 6a, which is supplied from the main grid. It is important to highlight that, the panel photovoltaic has a relevant role in the contribution of energy between the 10:00 and 18:00 hours, which coincides with the period of high irradiation, see Fig. 6c. It is clear that the power provided by the wind turbine has a similar shape than the wind speed shown in Fig. 6b. The battery experiences periods of charge ($P_{Bnj}^{t_z} < 0$) and discharge ($P_{Bnj}^{t_z} > 0$). In particular, it is possible to see that in periods with high wind power generation (e.g. at hours 4 and 10) the battery is charged ($P_{Bnj}^{t_z} < 0$). This power is useful to reduce the energy cost in hours of peak demand (e.g. at hours 13 and 20). This fact fits with the battery SOC shown in Fig. 7b

Figure 7c shows the cost in $/h of the total energy imported from the main grid. It is clear that the cost varies depending on the imported power from main grid and has its highest value around the 20 hour, which is

where the high peak demand happens. Moreover, in the same figure it is possible to compare the energy cost if there would be no renewable power sources, clearly, without renewable sources the energy cost increases.

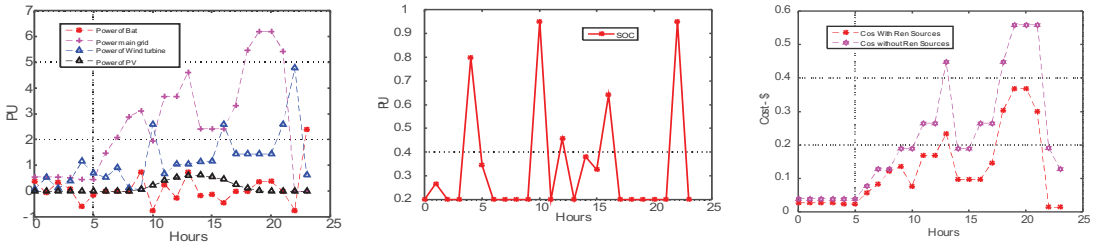

Fig. 7 Case study solved with the interior point method a) generated power b) battery SOC c) cost of the energy from the main grid

These results were obtained by means of the interior point method. In this work, the solution of this problem will be analyzed with the three different optimization methods explained in the section below.

6.1 Results of the different methods of optimization

To carry out this study, tests have been done taking into account the following points:

- It has been repeated several times the execution of each configuration and have taken into account all the results through the arithmetic mean and the standard deviation.
- It has been evaluated the most important parameters and those ones that fit better to this problem, maintaining fixed the rest.
- For each tool, it has been selected for this study those parameters that are relevant to the problem, setting the rest to their values by default.

6.1.1 Interior Point Method (fmincon)

Because this is a deterministic method for a given problem, its performance depends mainly of the initial condition. However, the initial condition for the OPF problem for the tertiary control of microgrids is completely defined, so arbitrary modification makes no practical sense. However, it is possible determine the CPU time required for the complete execution of the OPF analysis and the value of the objective function ("fitness") associated. The last results will serve as reference like comparison with them associated to them methods meta-heuristics. In this case, the convergence, the solution provided by the interior point method is associated to a fitness of $3 units currency, while the time of computation is of approximately 3630 s.

6.1.2. Direct Search (patternsearch)

As can observe in Figs. 8a and 8b for the parameter *Pollingorder* of the function *patternsearch*, the option *Consecutive* is the one that obtains best results in the fitness value. But, in cost time terms, the option that is the fastest is *Random*. On the other hand, Figs 9a and 9b show the effect of the parameter *Pollmethod*. In this case the option that gives best results for both, as in fitness values as at runtime, is *MADSPositiveBasisNp1* that is the option will be used during the optimization.

Fig. 8 Effect of *PollinfOrder* parameter: a) value of the fitness function b) time spent

Fig. 9 Effect of *PollMethod* parameter: a) value of the fitness function b) time spent

6.1.3. Genetic Algorithm (GA)

As is shown in Fig. 10a and 10b, in general to increase the population size gets a better result in the fitness value but, at the same time, it implies a higher computational time. Therefore, searching a tradeoff between fitness value and computational cost, the population size has been set to 25. Figure 11a and 11b show the evaluation of the parameter *selectionFCN* where is possible to see that for both, the fitness value and the computational cost, the best option is *selectiontournament*. Finally, in Figures 12a and 12b evaluate the parameter *crossoverFCN* where it is shown that the best result for the fitness value is the option *crossoverscartered* whereas the option *crossoverheuristic* is the best one in computational cost terms. Since in this work the execution time of the algorithm is a priority the last option, *crossoverheuristic*, will be selected.

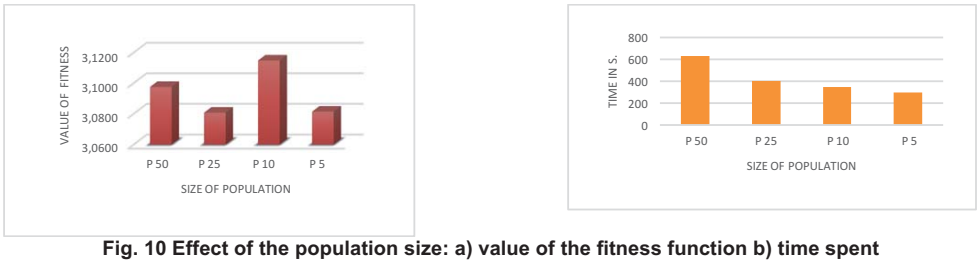

Fig. 10 Effect of the population size: a) value of the fitness function b) time spent

Fig. 11 Effect of *selectionFCN* parameter: a) value of the fitness function b) time spent

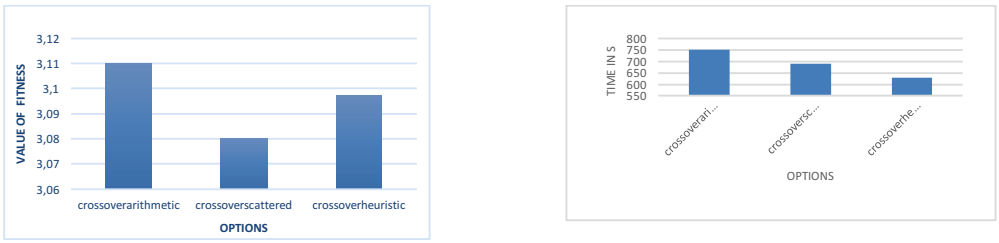

Fig. 12 Effect of *crossoverFCN* parameter: a) value of the fitness function b) time spent

6.1.4. Comparison of results between the different methods

As is possible to see in Fig. 14 the method that achieves the best result in the fitness value is the interior point through the *fmincon* function. In computational time terms the genetic algorithm method is the one that obtains a smaller computational cost. Finally, the direct search method through the *patternsearch* function is the one that gets a worst value for the fitness value and intermediate results in computational cost. Therefore, three different methods have been tested and can be used to solve the optimization problem of OPF in micro-grids each one with its advantages and disadvantages. It is important to note that, the interior point method is the one that best result obtains in the fitness function and its value will be used for continuous functions, but also, the genetic algorithm can solve not continuous fitness functions which is important since can evaluate cost functions which different behaviors between day and night.

Fig. 14 Comparison of the different optimization methods: a) value of the fitness function b) time spent

Figure 15 shows the results of the optimization of the microgrid presented in Fig. 5 with the three methods, Fig. 15a depicts the power of the main grid whereas Fig. 15b the costs of the imported power compared to the cost of the total energy load. It is important to highlight that, the solutions given for the three methods varying only in a percentage of 2% for the genetic algorithm and a percentage of 4% for the direct search method with respect to the interior point one.

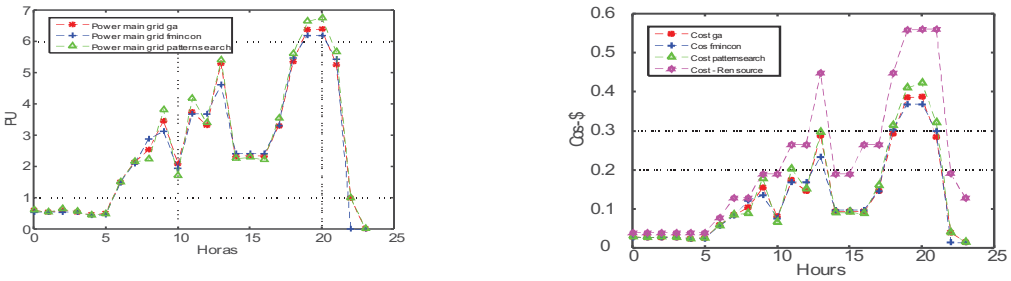

Fig. 15 Results obtained with the three optimization methods: a) Comparison of power main grid b) Comparison of cost of the imported power compared to the cost of the total energy load

7. Conclusions

In this work a model for the analysis of OPF microgrids is presented. The model allows us to manage the energy storage elements to improve the economic operation of the microgrid. Likewise, through it is possible to determine the optimal amount of power imported from the main grid. The model considers basic models of the elements of the distribution system, photovoltaic panels, wind turbines, as well as batteries for energy storage. The model is solved by three different optimization methods: i) interior point, ii) genetic algorithm and, iii) direct search. The presented numerical results illustrate the potential analysis of OPF to determine values that could be used as a reference by the secondary controller of a microgrid. In addition, the validation of the optimization methods has been performed through the evaluation of a case study which has been efficiently solved.

8. Acknowledgments

This work has been possible thanks to the collaboration of CONACYT in conjunction with the University of Guanajuato Mexico and the CIESOL center of the University of Almeria Spain. Luis O. Polaco Vásquez, Cristian A. Carreño Meneses, Alejandro Pizano Martínez are fellows of Universidad de Guanajuato and CONACYT. This work has been funded by grants from the Spanish Ministry of Economy and Competitiveness (TIN2015-66680-C2-1-R and ENERPRO DPI 2014-56364-C2-1-R), Junta de Andalucía (P11-TIC7176 and P12-TIC301). Juana López Redondo and José Domingo Álvarez Hervás are fellows of the Spanish ‘Ramón y Cajal’ contract program, co-financed by the European Social Fund.

9. References

Acha, E., Fuerte C. R., Ambriz H., Camacho C., 2004 "FACTS Modelling and Simulation in Power Network", 1nd ed., England: John Wiley & Sons LTD, 117-125.

Acosta R., Potencial eólico en México. Comisión Federal de Electricidad, México, [Online]. Available in: http://www.conae.gob.mx/work/sites/CONAE/

Bellini, A., Bifaretti, S., Iacovone, V., Cornaro, C., September 2009., "Simplified model of a photovoltaic module," in Applied Electronics, 2009. AE 2009, 1(47-51), 9-10.

Bidram, A., Davoudi, A., December 2012, "Hierarchical Structure of Microgrids Control System," in Smart Grid, IEEE Transactions on, 3(4), 1963-1976.

Bose, B.K., March 2010, "Global Warming: Energy, Environmental Pollution, and the Impact of Power Electronics," in Industrial Electronics Magazine, IEEE , 4(1), 6-17.

Doniz-Gonzales V.V, Montaño-Fernández, C., Espinosa-Bustamante E., September 2006, Prospectiva del Sector Eléctrico 2005–2014, Dirección General de Planificación Energética, México, [Online]. Available in: http://www.sener.gob.mx/webSener /Electrico_2005_2014.pdf

Gill, S., Kockar, I., Ault, G.W., January 2014, "Dynamic Optimal Power Flow for Active Distribution Networks," in Power Systems, IEEE Transactions on, 29(1), 121-131.

Katiraei, F., Iravani, R., Hatziargyriou, N., Dimeas, A., May-June 2008, "Microgrids management," in Power and Energy Magazine, IEEE, 6(3), 54-65.

Larsen, P., Energy Policy Toolkit on System Integration of Wind Power Experiences from Denmark. Low Carbon Transition Unit, Denmark, [Online]. Available in: http://www.ens.dk/.

Levron, Y., Guerrero, J.M., Beck, Y., August 2013, "Optimal Power Flow in Microgrids with Energy Storage," in Power Systems, IEEE Transactions on, 28(3), 3226-3234.

Olivares, D.E., Cañizares, C.A., Kazerani, M., July 2014, "A Centralized Energy Management System for Isolated Microgrids," in Smart Grid, IEEE Transactions on, 5(4), 1864-1875.

The MathWorks Inc., 2002, "Matlab Optimization Toolbox", Users Guide Version 2, [Online], Available in: http://www.mathworks.com.

The MathWorks Inc., 2013, "Genetic Algorithm and Direct Search Toolbox™ 2", Users Guide Version 2, [Online], Available in: http://cda.psych.uiuc.edu/matlab_pdf/gads_tb.pdf

Wang L., Yeh T., Lee W., Zhe C., May 2009., "Benefit Evaluation of Wind Turbine Generators in Wind Farms Using Capacity-Factor Analysis and Economic-Cost Methods," in Power Systems, IEEE Transactions on, 24(2), 692-704.

Zúñiga Haro P., 2006. "Analysis and control of a series compensator", Ph.D. dissertation, Dept. Electrical Power Systems, CINVESTAV Gdl., Guadalajara, México, [Online]. Available in: http://orion.gdl.cinvestav.mx/~jramirez/Tesis_pavel2006.pdf

Appendix

This appendix shows the parameters of the microgrid components which are the following:

Table A. 1. Number of nodes and the microgrid components

Node	Lines	Battery	Loads	WT	Panel S.V.	Node slack grid
8	6	1	1	1	1	1

Performance data of the microgrid components

$$P_{eolico} = 400\ w\ , -100 < Q_{eolico} > 150VA$$

$$P_{bateria} = 300\ w$$

$$P_{red} = 800\ , -100 < Q_{red} > 150VA$$

$$P_{panel\ solar} = 75\ w$$

Grid cost coefficients

$$a = 0.014, b = 0.020, c = 0.0060$$

Voltage general bounds

$$Min = 0.95\ pu, \qquad Max = 1.05\ pu$$

Table A. 2. feeders

Node sent	Node receiving		R (P.U.)	T (P.U.)	BC (P.U.)
3	2		0.00029	0.00086	0
4	3		0.00029	0.00086	0
5	4		0.00029	0.00086	0
1	2		0.00029	0.00086	0
6	3		0.00029	0.00086	0
5	8		0.00029	0.00086	0